ADVANCED ENERGY MATERIALS
www.advenergymat.de

Transition Metal Assisting Pre-Lithiation Reduces the P/N Ratio to Balance the Energy Density and Cycle Life of Aqueous Batteries

*Tianshi Lv, Xiangzhen Zhu, Zejing Lin, and Liumin Suo**

Aqueous Li-ion batteries (ALIBs) are safe, environmentally friendly, and cost-effective, promising for electric energy storage (EES). The high voltage ALIBs (HV-ALIBs) supported by water-in-salt electrolytes are ideal for lowering the energy cost ($/Wh) of EES. However, HV-ALIBs have been built with a high positive/negative capacity ratio (P/N ratio) to ensure their long-term cycle life due to the irreversible Li consumption in the initial cycle induced by the solid electrolyte interface (SEI) formation and the parasitic reaction. Thus, the benefits of HV-ALIBs in cost and energy density are mitigated inevitably. Generally, the feasible approach is adding per-lithiation additives (PAs) to compensate for the capacity loss in the initial cycle. However, using PAs in ALIBs is challenging due to the high chemical activity of water. Here, a new strategy to achieve the pre-lithiation by introducing manganese metal as a sacrificial PA for HV-ALIBs that can provide over 900 mAh g^{-1} specific capacity without any adverse impact is proposed. The P/N ratio reduces to 1.02 by the $LiMn_2O_4||TiO_2$ pouch cell using the sacrificial manganese PA. This results in a high initial energy density above 120 Wh kg^{-1} and outstanding cycle stability with a capacity retention of 80% after 400 cycles.

1. Introduction

Due to their high energy density and output voltage, rechargeable lithium-ion batteries dominated electric vehicles and portable electronics.[1–3] However, security issues are gradually emerging because of the flammability of the organic electrolytes, which can be a thorny barrier for the application in grid-scale energy storage and renewable energy storage.[4–7] High voltage aqueous Li-ion batteries (HV-ALIBs), which have recently been proposed as exhibiting a water-in-salt (WIS) electrolyte, are promising for electric energy storage (EES) because of their inherent safety and relatively high energy density.[8–10] However, similar to the traditional non-aqueous lithium-ion batteries (LIBs), the HV-ALIBs with WIS electrolytes also suffer from the initial irreversible capacity loss for forming the solid electrolyte interface (SEI) on the anode.[11–13] Additionally, before the SEI formed properly, hydrogen evolution was a natural side reaction, inevitably lowering the initial Coulombic efficiency (CE) and degrading the cycle life. Thus, compared to traditional non-aqueous LIBs, the initial irreversible capacity loss in ALIBs is more severe. Regarding this issue, the positive/negative capacity ratio (P/N ratio) plays a vital role in energy density and cycle life. Generally, the battery with the ideal P/N ratio of 1 exhibits the highest energy density, and the more deviation from the ideal value of 1, the lower the energy density would be. However, considering the influence of cycle life, over-charge/over-discharge, and other safety issues, in practice, the P/N ratio cannot be set to 1. The P/N ratio in ALIBs is much greater than 1 to compensate for the irreversible loss resulting from the SEI formation process and the parasitic reaction before the SEI formation, in contrast to the traditional non-aqueous LIBs, whose P/N ratio is often below 0.95 to prevent lithium dendrite precipitation.[14] Taking the $LiMn_2O_4||TiO_2$ system as an example, in which the initial CE is about 85%–90%, assuming that the excess $LiMn_2O_4$ compensates for all the initial irreversible capacity loss, the P/N ratio should be increased to 1.3. Besides, taking the irreversible capacity loss resulting from the formation of the SEI layer in the following cycles, it is reasonable to set up the P/N ratio close to 1.5. Therefore, according to all reported work, their P/N ratios are close to 1.5.[15–19]

However, the excessive cathode material lowers the energy density of full batteries; more specifically, a P/N ratio of 1.5 increases the mass weight of all electrodes above 20%, reducing the energy density by 30 Wh kg^{-1}. Conversely, a P/N

T. Lv, X. Zhu, Z. Lin, L. Suo
Beijing Advanced Innovation Center for Materials Genome Engineering
Key Laboratory for Renewable Energy
Beijing Key Laboratory for New Energy Materials and Devices
Beijing National Laboratory for Condensed Matter Physics
Institute of Physics
Chinese Academy of Sciences
Beijing 100190, China
E-mail: suoliumin@iphy.ac.cn
T. Lv, X. Zhu, Z. Lin, L. Suo
Center of Materials Science and Optoelectronics Engineering
University of Chinese Academy of Sciences
Beijing 100049, China
L. Suo
Yangtze River Delta Physics Research Center Co. Ltd
Liyang 213300, China
The ORCID identification number(s) for the author(s) of this article can be found under https://doi.org/10.1002/aenm.202202447.

DOI: 10.1002/aenm.202202447

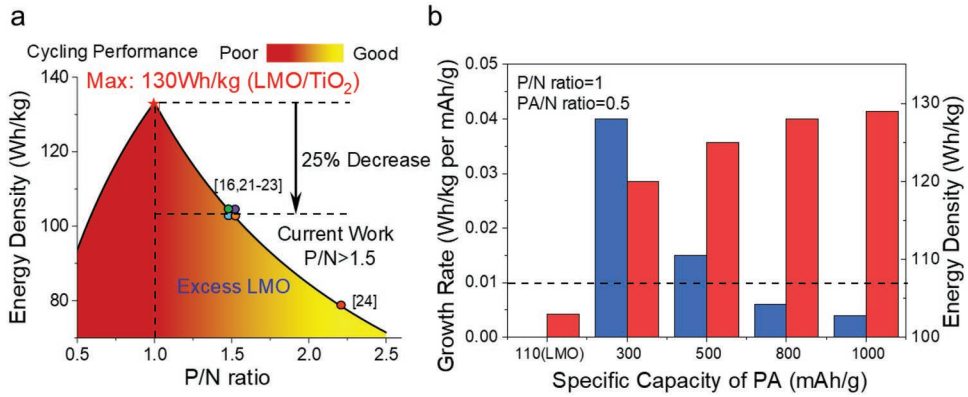

Figure 1. Influence of the P/N ratio and pre-lithiation additives on energy density and cycle life of HV-ALIBs ($LiMn_2O_4$/WIS/TiO_2). a) The varied P/N ratio impacts the energy density and cycling performance. b) The estimated energy densities with the varied specific capacities of PAs at the P/N ratio of 1 and PA/N ratio of 0.5.

ratio of up to 1.5 results in higher cost in cathode materials and the harsh fabrication of a thicker electrode, which lessens the cost-saving advantage of HV-ALIBs and increases production complexity. Therefore, compensating for the lithium loss in the initial cycle without increasing the P/N ratio is crucial for HV-ALIBs.

As traditional non-aqueous LIBs[20] taught us, adding properly designed pre-lithiation additives (PAs) to the electrodes to contribute active lithium is a simple and effective method to compensate for the initial irreversible capacity loss. Many sacrificial additives have so far been used in the traditional non-aqueous LIBs, including lithium powder, Li_3N, Metal/LiF, Li_2O, Metal/Li_2O, Li_2NiO_2, Li_6CoO_4, and so on.[21–25] However, unfortunately, almost all common PAs in traditional non-aqueous LIBs are unsuitable in ALIBs, because they not only demonstrate water solubility [22,23,26] but also demonstrate high chemical reactivity to the water, resulting in the degradation of the electrolyte and gas evolution.[25–28] Thus, up to now, an attempt at PAs for ALIBs barely exists, even though improving both the energy density and cycling performance is essential.

In this study, we proposed using a sacrificial transition metal as the cathode PA for ALIBs. The transition metal PA is a pure metal substance and does not contain lithium resources that are different from the traditional lithium-containing PAs. In the initial cycle, the transition metal PA is first oxidated to the corresponding ions into the electrolyte before charging the cathode to offer the adequate capacity to compensate for the irreversible loss of the anode. By this mechanism, the transition metal not only demonstrates high chemical stability in the water and good compatibility with the electrodes, but it also offers a high pre-lithiation specific capacity (theoretical value: > 900 mAh g^{-1}) by its own electrochemical oxidation, satisfying all the demands of PA in ALIBs. Its efficacy is successfully demonstrated in HV-ALIBs ($LiMn_2O_4$‖TiO_2). Impressively, using the sacrificial transition metal PA enables the reduction in the P/N ratio to 1.02 and well-balanced cycle life and energy density, whose capacity retention is over 80% after 400 cycles, and initial energy density of 121 Wh kg^{-1} based on the total electrode mass is higher 20% than of 100 Wh kg^{-1} in the condition of P/N 1.47 without PA.

2. Estimation of the Energy Density with the Varied P/N Ratio

As mentioned above, the P/N ratio demonstrates a significant impact on the performance of batteries. **Figure 1**a shows the relation between the P/N ratio and energy density, considering the cycling performance in the HV-ALIBs ($LiMn_2O_4$‖TiO_2). Considering the actual specific capacity of $LiMn_2O_4$ and TiO_2 (148 and 168 mAh g^{-1}, respectively) differs slightly from the theoretical value, 110 and 150 mAh g^{-1} are selected for the $LiMn_2O_4$ cathode and TiO_2 anode, respectively, whose highest energy density based on electrodes is 130 Wh kg^{-1}. Further, this demonstrates that as the P/N ratio deviates from the ideal value of 1, the energy density drops regardless of whether the excess of the cathode and the anode is higher or lower than the ideal value of 1. Due to more active lithium in the cathode to compensate for the initial irreversible capacity loss, the high P/N ratio is more favorable to lasting the cycle life compared with the excessive anode with a P/N ratio lower than 1. Thus, to balance the energy density and cycle life, in most studies about HV-ALIBs ($LiMn_2O_4$‖TiO_2), the mass ratio of the positive and negative electrodes is fixed at 2 (Table S1, Supporting Information). Correspondingly, the P/N ratio is 1.47,[15–17,19] whose energy density is reduced to only 100 Wh kg^{-1} in such a case. In other words, it shows that the P/N ratio demonstrates a significant role in determining the energy density and that the key practical challenge for HV-ALIBs is to attain a P/N ratio that is infinitesimally close to 1 without degrading cycle life.

While maintaining a higher energy density and improved cycling performance, the PAs can benefit from the high specific capacity in the initial cycle and offer ample active lithium with less mass. Next, we can regard the excess $LiMn_2O_4$ as a type of PA with a relatively low specific capacity and define the capacity ratio of PA and negative electrode as the "PA/N ratio" to indicate the amount of PA to visually evaluate the advantage of PA in energy density. To discuss how energy density changes by PAs of different specific capacities, we assume an ideal P/N ratio of 1 with the PA/N ratio of 0.5 based on the above rough estimation corresponding to the P/N ratio of 1.5 in previous literature (Figure 1b). For example, when the

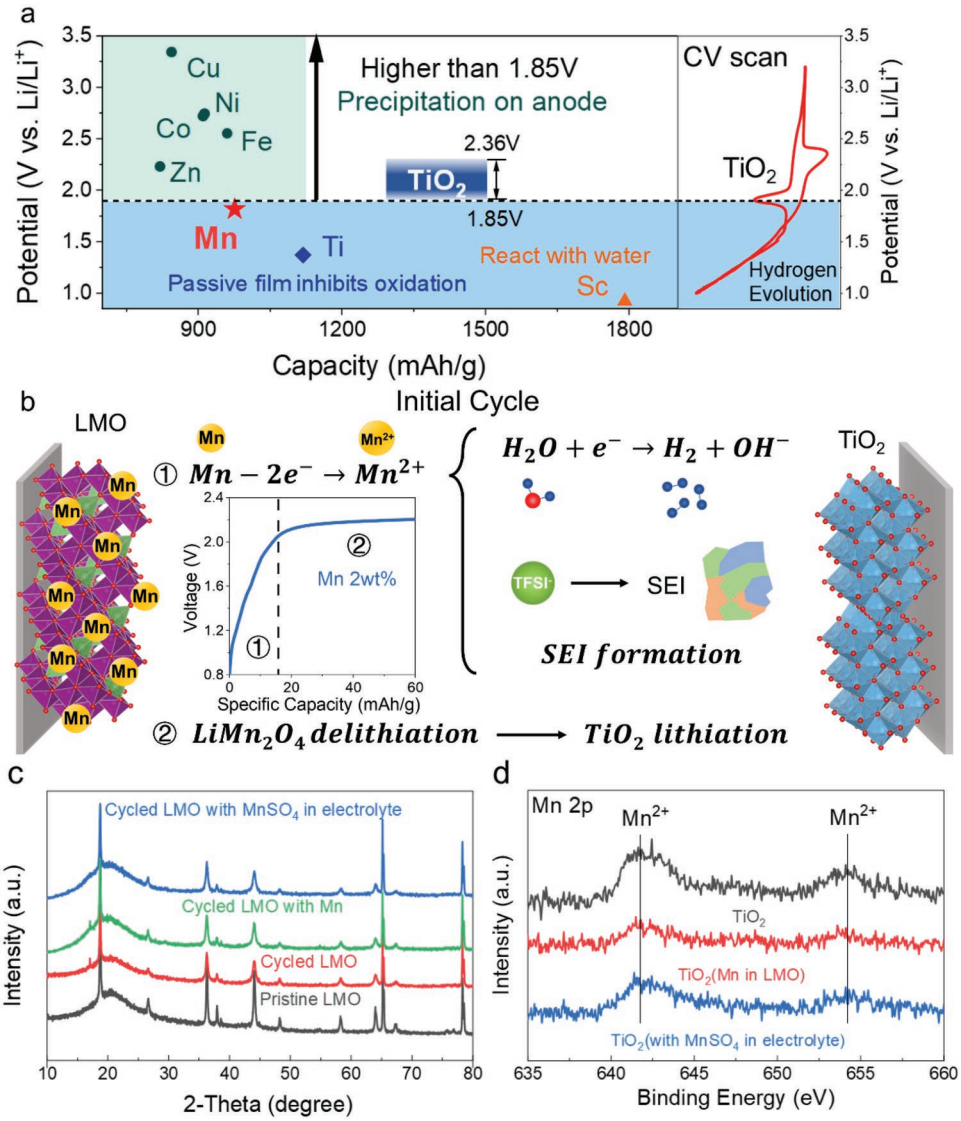

Figure 2. The proposal of manganese as PA for HV-ALIBs ($LiMn_2O_4$/WIS/TiO_2). a) The screen of transition metal-based PAs. b) The pre-lithiation mechanism of Mn. c) XRD patterns of pristine $LiMn_2O_4$, $LiMn_2O_4$ after 50 cycles, $LiMn_2O_4$ after 50 cycles in 20 m LiTFSI with saturated $MnSO_4$, and $LiMn_2O_4$ with Mn PA after 50 cycles. d) XPS spectrum of TiO_2 after 50 cycles, TiO_2 after 50 cycles in 20 m LiTFSI with saturated $MnSO_4$, and TiO_2 after 50 cycles.

specific capacity of PA is 110 mAh g^{-1}, whose effect is equivalent to excess $LiMn_2O_4$, the energy density is only 103 Wh kg^{-1}. As the specific capacity increases to 300 and 500 mAh g^{-1}, the energy density reaches 120 and 125 Wh kg^{-1}. After that, even if the specific capacity increases, the energy density barely changes and approaches the limit. When the specific capacity of PA is taken into account, the growth rate of the energy density is approximately 0.04 at 300 mAh kg^{-1}, meaning that when the specific capacity grows by 1 mAh g^{-1}, the energy density increases by 0.04 Wh kg^{-1}. However, when the specific capacity is higher than 500 mAh g^{-1}, this value decreases below 0.01. In such a case, the contribution of the PA barely changes with the increase in the specific capacity of the PA. As a result, we can say that PA's specific capacity of 500 mAh g^{-1} is sufficient to ensure that the high energy density of HV-ALIBs is greater than 125 Wh kg^{-1}.

3. Proposal of the Manganese Pre-Lithiation Additive

We believe that the transition metal group would be a potential group of options given that the PA of ALIBs is required to meet the condition of outstanding chemical stability in air and water and high oxidation-specific capacity. **Figure 2**a shows the oxidation potential and specific capacity of different transition metals. The electrochemical pair of $LiMn_2O_4$ and TiO_2 is fixed by the screening standards mentioned above. First, the oxidation potential should be below the redox potential of TiO_2 (1.85 V) to avoid the oxidation product of the transition metal (M^{z+}) being reduced and deposited on the surface of the TiO_2 anode. Thus, Cu, Co, Ni, Fe, and Zn metals are excluded here. Second, due to its lack of chemical stability in aqueous solutions, the Sc metal is disregarded. Third, due to failure to ensure a continuous

sacrificial reaction, the Ti metal is also excluded. It is easily oxidated into dense titanium oxide passivation film, stopping its further oxidation. Therefore, finally, Mn metal stands out as the PA for ALIBs. Manganese shows unique advantages, including high chemical stability in the aqueous electrolytes, higher oxidation-specific capacity ($Mn - 2e^- \rightarrow Mn^{2+}$, 976 mAh g^{-1}) that exceeds our estimated minimum demand value (500 mAh g^{-1}), and lower reduction potential of 1.815 V versus Li/Li^+ than the redox peak of TiO_2 (1.85 V). All those characteristics ensure it is an ideal candidate for PA. In experiments, we mix Mn metal powder into the active cathode material, binder, and carbon black to make the pre-lithiation cathode (Figure S1, Supporting Information), which is easy to produce even in an air environment. Next, Figure 2b shows the schematic of the Mn metal PA mechanism. During the charging process for the first cycle, on the cathode side, the Mn PA in the cathode is first electrochemically oxidized to Mn^{2+} dissolved into the electrolyte before the de-lithiation of the $LiMn_2O_4$ cathode due to the low oxidation potential of Mn. Correspondingly, on the anode side, SEI formation and the parasitic reaction of hydrogen evolution coincide with the oxidation of Mn PA, consuming the capacity supplied by Mn PA and maintaining a charge balance. After most of the Mn PA is consumed, as the voltage increases, the delithiation of $LiMn_2O_4$ and the lithiation of TiO_2 normally begin, during which the Mn exists in the electrolyte as ions.

The structural stability of $LiMn_2O_4$ cathodes with/without Mn additive is verified by the X-ray diffraction (XRD) pattern (Figure 2c), including pristine $LiMn_2O_4$ cathode, $LiMn_2O_4$ cathode cycled in WIS electrolyte (21 m LiTFSI), $LiMn_2O_4$ cathode cycled in 20 m LiTFSI electrolyte with saturated $MnSO_4$, and $LiMn_2O_4$ cathode with Mn PA cycled in WIS electrolyte. It shows that the structure of $LiMn_2O_4$ cathodes maintains very well after the introduction of Mn PA or Mn ion-containing electrolyte, indicating no matter Mn metal in the cathode or dissolving into the electrolyte after pre-lithiation does not exhibit any negative impact on the structural stability of the $LiMn_2O_4$ cathode. Also, the morphologies of cycled $LiMn_2O_4$ electrodes with Mn PA and TiO_2 electrodes almost keep them pristine before and after cycled (Figures S2 and S3, Supporting Information). Furthermore, to justify that the dissolved Mn ion in the electrolyte is impossible to re-deposit on the anode side, we also performed the Mn 2p XPS on the TiO_2 anode. As Figure 2d shows, the cycled TiO_2 anodes after 50 cycles only reveal strong peaks of Mn^{2+} without any peak at 650 eV belonging to Mn metal, manifesting that the re-deposition of Mn metal can not occur on the surface of the TiO_2 anode. Meanwhile, our claim is double-checked by the cyclic voltammogram results of TiO_2 anode in 21 m LiTFSI and 20 m LiTFSI with saturated $MnSO_4$ with the cut-off voltage at −1.4 V versus Ag/AgCl that fail to detect the reduction peak for Mn^{2+} (Figure S4, Supporting Information). Besides, the C 1s and F1s XPS spectrums of cycled TiO_2 anodes are also performed to clarify that Mn PA would not impact the SEI formation in the full batteries (Figure S5, Supporting Information). The minor peak at 684.5 eV in F 1s spectra was assigned to LiF, which originated from reduced $TFSI^-$.[29] The positions and shapes of the peaks in both the pre-lithiation and non-pre-lithiation groups are almost the same, meaning that the addition of Mn PA has little influence on the SEI formation. To explore the existing form of divalent Mn in cycles, the simulated cycled electrolyte was obtained by electrochemical oxidation of the Mn electrode in 21 m LiTFSI. After the electrochemical oxidation of Mn in it, the appearance of the electrolyte only changes a little. However, when NaOH solution is added to the electrolyte, it turns turbid (Figure S6a, Supporting Information), meaning that the divalent Mn exists in the Mn^{2+} form in the electrolyte. If the above solution with Mn^{2+} is taken to test the electrochemical stability compared with 21 m LiTFSI, there is no obvious difference between the linear sweep voltammetric curves (Figure S6b, Supporting Information). We can conclude that Mn metal is an ideal sacrificial transition metal PA with a proper oxidation potential based on the above results, high specific capacity, high chemical stability in aqueous electrolytes, and good compatibility in aqueous batteries, satisfying all the demands of the PA for ALIBs.

4. Pre-Lithiation Effect Verification and Optimization of the Manganese

The amount of Mn additive that should be utilized as PA in the HV-LIBs (the $LiMn_2O_4$‖TiO_2 batteries) with a P/N ratio of 1.02 is optimized in this work. The mass ratio of Mn to TiO_2 should be about 1.7–2.6 wt% based on the theoretical specific capacity of Mn additive (976 mAh g^{-1}), assuming the compensation for the initial irreversible capacity loss (10–15%) in the first cycle. Thus, calculated by the P/N ratio of 1.02, the mass fractions in the cathode of 1, 2, and 5 wt% are selected to study the effect of Mn content (**Figure 3**).

As Figure 3a shows, compared with the initial charging curve of the non-pre-lithiation cathode, the pre-lithiation cathodes with 1 wt%, 2 wt%, and 5 wt% Mn additive in WIS electrolyte (21 m LiTFSI) show extra capacity contributions from the Mn electrochemical oxidation in the voltage range of 0.8–2.0 V in the first charging, recognizing approximately 3 mAh g^{-1} for 1 wt%, 10 mAh g^{-1} for 2 wt%, and 30 mAh g^{-1} for 5 wt%, respectively. Furthermore, to verify the Mn pre-lithiation, the pure Mn cathode without $LiMn_2O_4$ is paired with the TiO_2 anode (Figure S7, Supporting Information). It shows that the TiO_2 anode is charged by Mn, proving that the Mn additive can work as the PA in the first cycle. However, the Mn content in the cathode is not the more, the better. Figure 3a also gives corresponding complete initial charge/discharge curves, showing that the initial discharge-specific capacity at 1 V is much lower in the Mn 5 wt% than in the other 1 and 2 wt%. It is inevitable to make the $LiMn_2O_4$ over-lithiation seriously in the following discharging because, in the Mn 5 wt%, the anode has been filled with the redundant capacity of excess Mn additive, which could affect the subsequent cycling performance. However, in the Mn 2 wt%, the capacity of Mn additive is nearly all used to make up for the irreversible loss, so little over-lithiation occurs. Figure 3b shows the cycling performances of those full batteries, confirming that the Mn 5 wt% demonstrates the worst cycling performance, resulting from the excess Mn PA and $LiMn_2O_4$ over-lithiation. Also, insufficient capacity is found in the Mn 1 wt%, resulting in faster cycle decay than the Mn 2 wt%. Hence, the optimal amount of Mn additive is 2 wt% because the 2 wt% is probably just right to compensate for the

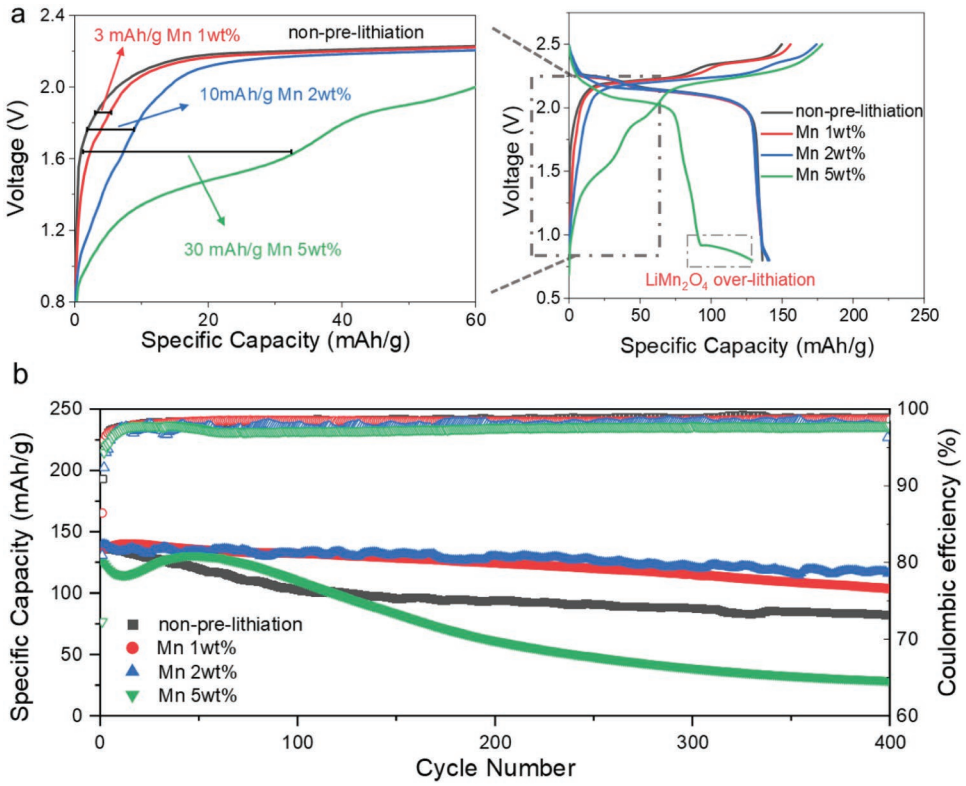

Figure 3. The pre-lithiation performance verification of Mn additive in $LiMn_2O_4||TiO_2$ ALIBs. a) The initial voltage profiles and the enlarged view of the initial charge profiles of $LiMn_2O_4||TiO_2$ full batteries with different amounts of the Mn additive in $LiMn_2O_4$ cathode. b) Cycling stability and CE of $LiMn_2O_4||TiO_2$ full batteries with different amounts of the Mn additive in $LiMn_2O_4$ cathode.

capacity loss in the initial cycles, realizing better cycling performance.[30,31] The leakage current characteristics of full batteries with or without Mn 2 wt% reveals that introducing Mn^{2+} does not increase the leakage current (Figure S8, Supporting Information). Moreover, the rate performance at different current densities for five cycles of the Mn 2 wt% pre-lithiation full battery was provided in Figure S9, Supporting Information. The high discharge capacity of 141, 131, 115, and 97 mAh g^{-1} at current densities of 1, 2, 5, and 10 C were obtained, indicating its good rate of performance. The Mn 2p XPS spectrum of the above TiO_2 anode has been provided in Figure S9, Supporting Information, proposing a similar peak position to the results in Figure 3d, demonstrating that even at high current densities, the Mn^{2+} is impossible to be reduced and deposited on the surface of TiO_2. Based on these results, we finally choose the Mn 2 wt% as the reasonable amount of Mn additive used in the following experiments.

Figure 4 shows that the $LiMn_2O_4||TiO_2$ full batteries with the various P/N ratios (1.02, 1.47, and 2.2) are controlled by the mass ratio of positive and negative electrodes precisely, whose conversion relations are listed in Table S2, Supporting Information. Figure 4a shows their attainable energy densities with a cycle life of more than 400 times. When the P/N ratio is close to 1, it shows that the P/N 1.02 demonstrates the highest initial energy density of 122 Wh kg^{-1} based on the total electrode mass; however, without the excessive Li supplement from the $LiMn_2O_4$ cathode, its cycle will decay severely, whose capacity retention is lower than 40% after the 400 cycles. In contrast, when the P/N ratio is 1.47 as previous literature used or increased to 2.2, the cycle fading issue can be resolved effectively with the high capacity retention of more than 90% after 400 cycles (Figures S10 and S11, Supporting Information). Still, the energy density of the P/N 1.47 is no more than 100 Wh kg^{-1} and even below 80 Wh kg^{-1} in the P/N 2.2. Thus, balancing both energy density and cycle life is difficult if we do not apply the Mn PA. Figure 4b shows the cycle stability employing 2 wt% Mn additive at the P/N ratio of 1.02. Impressively, compared with the control sample without the Mn additive, the introduction of 2 wt% Mn additive demonstrates a high energy density of 121 Wh kg^{-1}, very close to our estimated maximum value of 130 Wh kg^{-1}. Additionally, it exhibits superior cycle stability, whose energy density remains around 100 Wh kg^{-1} at the 400^{th} cycle, fully reflecting the advantage of Mn PA. To further demonstrate the advantages of Mn additive, in Figure 4c we summarized the energy densities (Wh kg^{-1}) based on the total electrode mass and energy density decay rate (ED decay rate: %/cycle) with the different P/N ratios of 1.02, 1.47, and 2.2. After using Mn PA, the energy density decay rate at the P/N ratio of 1.02 is reduced by more than 60%, from 0.1% to 0.03%, achieving a well-balance between energy density and cycle life.

To further demonstrate the effectiveness of our Mn PA, the hand-made single-layer mAh level pouch cells (capacity: 13.5 mAh, 3 × 4 cm, P/N ratio = 1.05) are assembled. As the first charge-discharge profile shown in Figure 4d, at such a low P/N

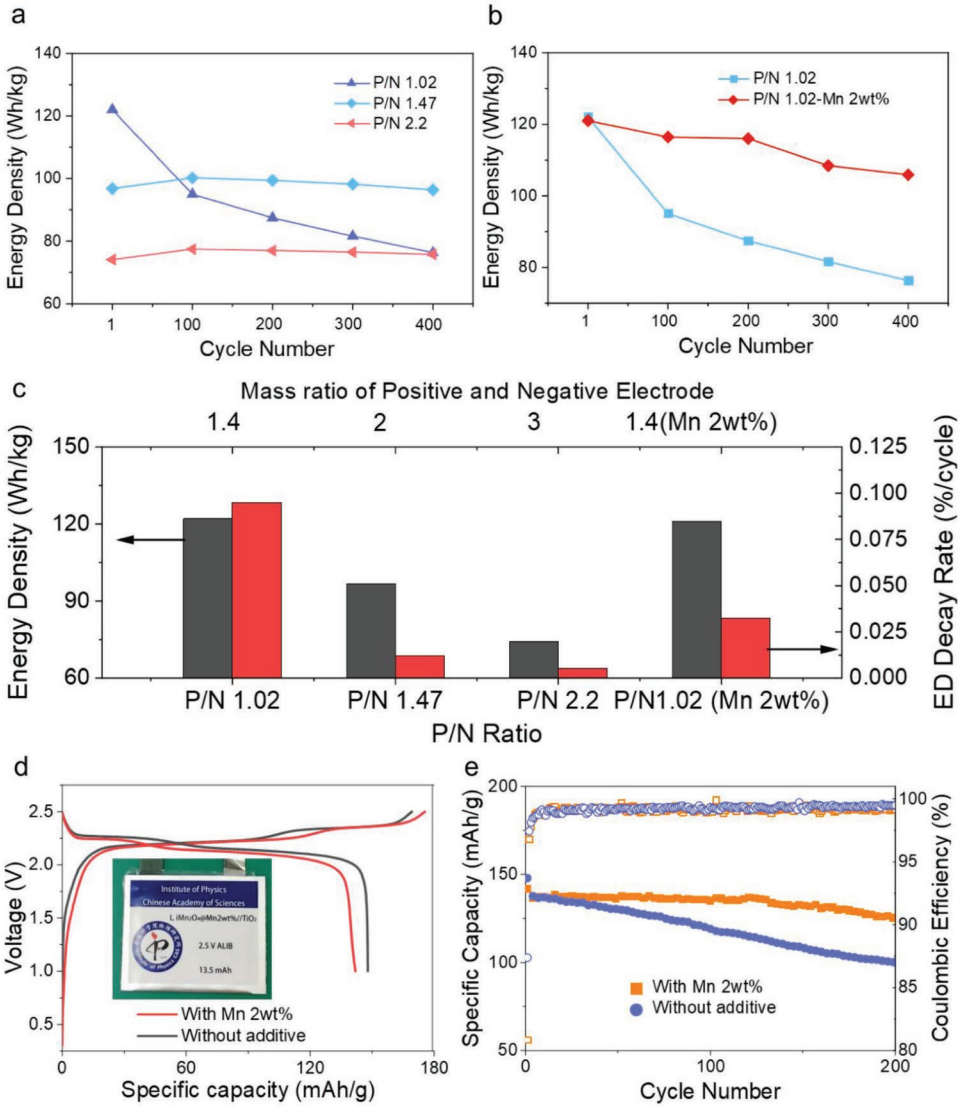

Figure 4. The effect of Mn PA on the energy density and cycling performance of ALIBs in a low P/N ratio. a) The cycling performance of $LiMn_2O_4$||TiO_2 full batteries in different P/N ratios. b) The cycling performance of $LiMn_2O_4$||TiO_2 full batteries in P/N ratio of 1.02 with and without 2 wt% Mn PA. c) The energy density at the 5th cycle and energy density decay rate of the $LiMn_2O_4$||TiO_2 full batteries in different P/N ratios and $LiMn_2O_4$||TiO_2 full battery with 2 wt% Mn PA in P/N ratio of 1.02. d) The initial voltage profile and e) the cycling performance of $LiMn_2O_4$||TiO_2 pouch cell (13.5 mAh) at an areal capacity of 1.1 mAh cm^{-2} with and without 2 wt% Mn PA.

ratio, both exhibit over 125 Wh kg^{-1} initial energy density based on the total electrode mass. However, the pouch cell with 2 wt% Mn PA shows higher capacity retention of 91.7% than 75% without 2 wt% Mn PA at the 200th cycle (Figure 4e), showing that the Mn PA demonstrates an excellent expansibility for scale-up applications. In a word, Mn pre-lithiation enables the P/N ratio to close to 1, which is very important for HV-ALIBs to demonstrate well-balanced energy density and cycling life.

5. Conclusion

We proposed the transition metal manganese as a novel ideal PA for HV-ALIBs. It exhibits a low oxidation potential (below 1.85 V vs Li/Li$^+$), a high pre-lithiation specific capacity (976 mAh g^{-1}), and great compatibility with all HV-ALIB components. Instead of using a much higher P/N ratio than 1, which is frequently used in previous studies, manganese added to $LiMn_2O_4$ cathodes with a P/N ratio close to 1 can contribute enough capacity to compensate for the initial irreversible loss in HV-ALIBs, avoiding the issues of low energy density caused by high P/N ratio and creating an outstanding balance between energy density and cycle life. In the $LiMn_2O_4$-TiO_2 full batteries, the P/N 1.02 group with 2 wt% Mn additives reaches the highest energy density of 121 Wh kg^{-1} with high capacity retention over 80% after 400 cycles. Therefore, our proposed transition metal pre-lithiation cathode additive would be promising for achieving an overall performance index, including high energy density, long-term cycle life, easy scale-up, and low cost.

6. Experimental Section

Materials Preparation: The lithium bis(trifluoromethane sulfonyl) imide (LiTFSI) was purchased from Shandong Hirong Power Supply Materials Co.LTD. The $LiMn_2O_4$ was purchased by MTI corporation, and the TiO_2 nanopowder was purchased from Sigma. Next, the WIS aqueous electrolyte (21 m LiTFSI) was prepared at the desired molalities (moles salt in kilogram solvent).

Characterization: XRD pattern of $LiMn_2O_4$ samples was obtained using an X-ray diffractometer (Brook Technology Co. LTD.) with Cu Kα radiation (the λ was 0.15405 nm) at the scan range of 10°–80°. The XPS analysis was performed by an ESCALAB 250 Xi, ThermoFisher with Mg/Al K αradiation. All the binding energies were referenced to the C1s line at 284.8 eV.

Electrochemical Measurements: $LiMn_2O_4$(Mn xwt%) and TiO_2 electrodes were prepared by well-mixed carbon black (CB) and PVDF (50 mg/mL) in N-methyl pyrrolidone (NMP) solvent, with the weight ratios of 8:1:1(80-x:x:1:1) and 7:2:1, respectively. All the slurry mixtures of $LiMn_2O_4$ and TiO_2 were coated on Al foil. After coating, the electrodes were removed to 55 °C for 2 h oven to remove the NMP, and then, they were cut into 0.785 cm^2 sheets. The mass loading of TiO_2 and $LiMn_2O_4$ was 3 and 4 mg cm^{-2} in the small pouch cell. The separator used in this work was Whatman glass fiber. Titanium mesh (80 mesh) coated with carbon film was used as the current collector for the cathode, and aluminum mesh (200 mesh) for the anode. To measure the electrochemical performance, the small pouch cell was used. In the pouch cell, the mass loading of TiO_2 and $LiMn_2O_4$ was about 7.5 and 10.7 mg cm^{-2}. The three-electrode cell of TiO_2 consisted of a TiO_2 work electrode, platinum mesh as the counter electrode, and Ag/AgCl as the reference electrode. The CV test was carried out on the CHI660E electrochemical working station. The galvanostatic charge/discharge tests were performed on a Netware battery test system (Shenzhen, China).

Supporting Information

Supporting Information is available from the Wiley Online Library or from the author.

Acknowledgements

This work is supported by the National Natural Science Foundation of China (51872322) and the Center for Clean Energy.

Conflict of Interest

The authors declare no conflict of interest.

Data Availability Statement

The data that support the findings of this study are available from the corresponding author upon reasonable request.

Keywords

aqueous lithium batteries, pre-lithiation additives

Received: July 18, 2022
Revised: August 24, 2022
Published online:

[1] J.-M. Tarascon, M. Armand, in *Materials for Sustainable Energy: A Collection of Peer-Reviewed Research and Review Articles from Nature Publishing Group* (Ed: V. Dusastre), World Scientific, Hackensack, NJ **2011**, pp. 171–179.
[2] M. Armand, J.-M. Tarascon, *Nature* **2008**, *451*, 652.
[3] J. B. Goodenough, Y. Kim, *Chem. Mater.* **2010**, *22*, 587.
[4] B. Dunn, H. Kamath, J.-M. Tarascon, *Science* **2011**, *334*, 928.
[5] K. Xu, *Chem. Rev.* **2004**, *104*, 4303.
[6] A. Hammami, N. Raymond, M. Armand, *Nature* **2003**, *424*, 635.
[7] L. Hu, K. Xu, *Proc. Natl. Acad. Sci. U. S. A.* **2014**, *111*, 3205.
[8] L. Suo, O. Borodin, T. Gao, M. Olguin, J. Ho, X. Fan, C. Luo, C. Wang, K. Xu, *Science* **2015**, *350*, 938.
[9] C. Yang, J. Chen, X. Ji, T. P. Pollard, X. Lü, C.-J. Sun, S. Hou, Q. Liu, C. Liu, T. Qing, Y. Wang, O. Borodin, Y. Ren, K. Xu, C. Wang, *Nature* **2019**, *569*, 245.
[10] J. Xu, X. Ji, J. Zhang, C. Yang, P. Wang, S. Liu, K. Ludwig, F. Chen, P. Kofinas, C. Wang, *Nat. Energy* **2022**, *7*, 186.
[11] L. Suo, D. Oh, Y. Lin, Z. Zhuo, O. Borodin, T. Gao, F. Wang, A. Kushima, Z. Wang, H.-C. Kim, Y. Qi, W. Yang, F. Pan, J. Li, K. Xu, C. Wang, *J. Am. Chem. Soc.* **2017**, *139*, 18670.
[12] N. Dubouis, P. Lemaire, B. Mirvaux, E. Salager, M. Deschamps, A. Grimaud, *Energy Environ. Sci.* **2018**, *11*, 3491.
[13] J. Yue, J. Zhang, Y. Tong, M. Chen, L. Liu, L. Jiang, T. Lv, Y.-S. Hu, H. Li, X. Huang, L. Gu, G. Feng, K. Xu, L. Suo, L. Chen, *Nat. Chem.* **2021**, *13*, 1061.
[14] C.-S. Kim, K. M. Jeong, K. Kim, C.-W. Yi, *Electrochim. Acta* **2015**, *155*, 431.
[15] L. Suo, O. Borodin, W. Sun, X. Fan, C. Yang, F. Wang, T. Gao, Z. Ma, M. Schroeder, A. von Cresce, S. M. Russell, M. Armand, A. Angell, K. Xu, C. Wang, *Angew. Chem., Int. Ed.* **2016**, *128*, 7252.
[16] M. R. Lukatskaya, J. I. Feldblyum, D. G. Mackanic, F. Lissel, D. L. Michels, Y. Cuie, Z. Bao, *Energy Environ. Sci.* **2018**, *11*, 2876.
[17] X.u Hou, R. Wang, X. He, T. P. Pollard, X. Ju, L. Du, E. Paillard, H. Frielinghaus, L. C. Barnsley, O. Borodin, K. Xu, M. Winter, J. Li, *Angew. Chem., Int. Ed.* **2021**, *60*, 22812.
[18] M. Turgeman, V. Wineman-Fisher, F. Malchik, A. Saha, G. Bergman, B. Gavriel, T. R. Penki, A. Nimkar, V. Baranauskaite, H. Aviv, M. D. Levi, M. Noked, D. T. Major, N. Shpigel, D. Aurbach, *Cell Rep. Phys. Sci.* **2022**, *3*, 100688.
[19] X. Hou, T. P. Pollard, W. Zhao, X. He, X. Ju, J. Wang, L. Du, E. Paillard, H. Lin, K. Xu, O. Borodin, M. Winter, J. Li, *Small* **2022**, *18*, 2104986.
[20] L. Jin, C. Shen, Q. Wu, A. Shellikeri, J. Zheng, C. Zhang, J. P. Zheng, *Adv. Sci.* **2021**, *8*, 2005031.
[21] Y. Sun, H.-W. Lee, Z. W. Seh, N. Liu, J. Sun, Y. Li, Y. Cui, *Nat. Energy* **2016**, *1*, 15008.
[22] K. Park, B.-C. Yu, J. B. Goodenough, *Adv. Energy Mater.* **2016**, *6*, 1502534.
[23] A. Abouimrane, Y. Cui, Z. Chen, I. Belharouak, H. B. Yahia, H. Wu, R. Assary, L. A. Curtiss, K. Amine, *Nano Energy* **2016**, *27*, 196.
[24] J. Du, W. Wang, A. Y. Sheng Eng, X. Liu, M. Wan, Z. W. Seh, Y. Sun, *Nano Lett.* **2019**, *20*, 546.
[25] M. Noh, J. Cho, *J. Electrochem. Soc.* **2012**, *159*, A1329.
[26] B. B. Fitch, M. Yakovleva, Y. Li, I. Plitz, A. Skrzypczak, F. Badway, G. G. Amatucci, Y. Gao, *ECS Trans.* **2007**, *3*, 15.
[27] M. G. Kim, J. Cho, *J. Mater. Chem.* **2008**, *18*, 5880.
[28] W. M. Dose, C. Villa, X. Hu, A. R. Dunlop, M. J. Piernas-Muãoz, V. A. Maroni, S. E. Trask, I. Bloom, V. Dravid, C. S. Johnson, *J. Electrochem. Soc.* **2020**, *167*, 160543.
[29] F. Wang, O. Borodin, M. S. Ding, M. Gobet, J. Vatamanu, X. Fan, T. Gao, N. Eidson, Y. Liang, W. Sun, S. Greenbaum, K. Xu, C. Wang, *Joule* **2018**, *2*, 927.
[30] L. Yu, Y. Tian, Y. Xing, C. Hou, Y. Si, H. Lu, Y. Zhao, *Ionics* **2021**, *27*, 5021.
[31] V. V. Kosilov, A. V. Potapenko, S. A. Kirillov, *J. Solid State Electrochem.* **2017**, *21*, 3269.